Development of force displaying device using pneumatic parallel manipulator and application to palpation motion

Masahiro Takaiwa
Okayama University

Toshiro Noritsugu
Okayama University

Proceedings of the 2003 IEEE
International Conference on Robotics & Automation
Taipei, Taiwan, September 14-19, 2003

Development of Force Displaying Device Using Pneumatic Parallel Manipulator and Application to Palpation Motion

Masahiro Takaiwa
Department of Systems Engineering,
Okayama University, 3-1-1 Tsushimanaka,
Okayama, 700-8530, Japan

Toshiro Noritsugu
Department of Systems Engineering,
Okayama University, 3-1-1 Tsushimanaka,
Okayama, 700-8530, Japan

***Abstract*— The goal of this study is to develop a mechanical system which display elastic characteristic like stiffness on the surface of human body aiming at applying to palpation simulator. Pneumatic parallel manipulator is employed as a driving mechanism, consequently, it brings capability of minute force displaying property owing to the air compressibility. Compliance control system without using force/moment sensor is constructed by introducing a disturbance observer and a compliance display scheme is proposed. The validity of the proposed scheme is verified experimentally.**

I. INTRODUCTION

A palpation motion is one of the most important medical examination to find a human disease like a cancer of the breast. There is a great need for the development of a mechanical system as a palpation training simulator[1] or a displaying device for remote diagnosis[2]. In this study we aim at developing a mechanical system which can display compliance characteristic of human skin, such as, "stiffness" for the operator's palpation motion(pushing at a point or slide on the surface) as shown in Fig.2.

A pneumatic parallel manipulator is employed as our displaying device since it can drive a multiple d.o.f. for its compactness due to the parallel link mechanism and it can execute minute force regulation owing to the air compressibility of pneumatic actuator which is indispensable feature for the palpation motion. The air compressibility simultaneously implies a feature of safety and softness, which are indispensable for the mechanical system contact with human directly.

In order to display a concrete compliance feeling to an operator, a control strategy is proposed where the applied force from an operator is estimated with no use of force/moment sensor and the contact point on which an operator is touching is detected based on that estimated force and finally realize a corresponding compliance by constructing a compliance control system[3]. By regulating the reference compliance value according to the movement of a contact point(motion of the finger), a palpation action is realized. The validities of the proposed control systems are confirmed through some experiments and analysis.

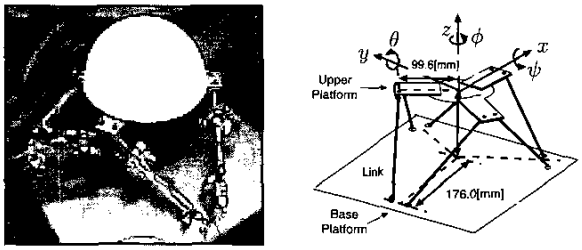

(a) Parallel Link Mechanism

(b) Pneumatic Driving Circuit

Fig. 1. Developed Pneumatic Parallel Manipulator

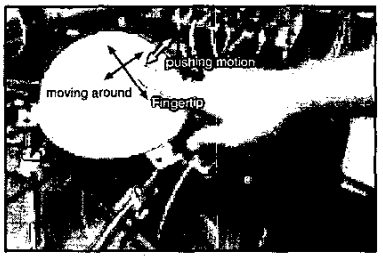

Fig. 2. Concept image of compliance display

II. OUTLINE OF PNEUMATIC PARALLEL MANIPULATOR

Fig. 1 (a) shows the developed pneumatic parallel manipulator. 6 pneumatic cylinders are employed to form so called Stewart type platform[4].

The position/orientation of the upper platform is expressed by a hand vector $\boldsymbol{h} = [x, y, z, \phi, \theta, \psi]^T$ using roll-pitch-yaw angle notation. The origin of hand coordinate frame $\boldsymbol{h}$ is set at a center point of upper platform when manipulator stands in a standard posture.

TABLE I

SYSTEMS PARAMETERS

T_p	Time constant of pressure response
T_{pn}	Nominal time constant of pressure response
k_p	Steady gain of pressure response
k_{pn}	Nominal steady gain of pressure response
k_v	Steady gain between piston velocity and pressure
m	Equivalent mass for one cylinder
b	Viscous coefficient
f_e	External force applied on a link
A_1, A_2	cross sectional area of cylinder chamber
p_1, p_2	air pressure in chamber
ℓ	displacement of piston rod
J	Jacobian matrix
T_q, T_{pq}	Time constant of filter

Similarly a link vector is defined as $\boldsymbol{\ell} = [\ell_a, ..., \ell_f]^T$ with an element of a displacement of each piston rod. Force/moment vector works at an origin of $\boldsymbol{h}$ is defined as $\boldsymbol{f_m} = [f_x, f_y, f_z, \tau_\phi, \tau_\theta, \tau_\psi]^T$. The equivalent force vector acts on piston rod is denoted with $\boldsymbol{f_e}$ which satisfy the following relation.

$$\boldsymbol{f_m} = \boldsymbol{J}^T \boldsymbol{f_e} \tag{1}$$

, where $\boldsymbol{J}$ is Jacobian matrix and it forms the next relation in a parallel manipulator mechanism.

$$\frac{d\boldsymbol{\ell}}{dt} = \boldsymbol{J}\frac{d\boldsymbol{h}}{dt} \tag{2}$$

In the mean while, Fig.1(b) shows the pneumatic driving circuit of one cylinder. Low friction type pneumatic cylinder is employed (Airpel Co. Ltd., 9.3mm in internal diameter, 50mm in rod stroke). Pressure in each cylinder's chamber, p_1, p_2 are detected by pressure sensors and the displacement of piston rod ℓ is measured by wire type linear encoder. The A/D converter is of 12 bit resolution.

A control signal u calculated every sampling period(10 ms) in a computer corresponds to an input voltage of a servo valve (FESTO, 50 ℓ/min) through D/A converter(resolution of 12 bit), which regulates the difference pressure of each cylinder. Supply pressure p_s is set to be 400 kPa. Table I shows the control parameters.

The linearized state equations of pressure in cylinder's chamber are described by the following equation[5].

$$T_p\frac{dp_1}{dt} = -p_1 + k_p u - k_v\frac{d\ell}{dt} \tag{3.a}$$

$$T_p\frac{dp_2}{dt} = -p_2 - k_p u + k_v\frac{d\ell}{dt} \tag{3.b}$$

Equation of motion of piston rod is expressed by Eq.(4).

$$p_1A_1 - p_2A_2 = f_g = m\frac{d^2\ell}{dt^2} + b\frac{d\ell}{dt} + f_e \tag{4}$$

III. RECOGNITION OF ELASTIC CHARACTERISTIC

A. Conceptional image

Fig.2 shows the concept image of compliance display. Human touches at an any point on the surface of an manipulator with their fingertip and implements a palpation motion by applying force for a various direction. The manipulator displays a corresponding force for the pushing motion of a fingertip by regulating compliance of the manipulator itself based on the displacement of fingertip and applied force. In order to realize such an action, a manipulator should have a function to detect which point a fingertip is pushing at and how much force is being applied. In the next section the strategy of compliance display including these detecting function is described.

B. Compliance control system

Fig.3 shows the proposed position based compliance control system[6]. The inner position control system is designed in order that the closed loop transfer function may follow the 3rd order system shown in Eq.(5).

$$\frac{\boldsymbol{H}}{\boldsymbol{H_r}} = \boldsymbol{G_r} = diag\left\{\frac{C}{s^3 + As^2 + Bs + C}\right\} \tag{5}$$

The inner block with a doublet represents a control system of generating force F_g as shown in Fig.4, which works to lower the influence of piston rod velocity that acts as disturbance on pressure response as shown in Eq.(3) as well as to make F_g to follow to the reference value with time constant T_{pn}[6].

First of all, the applied external force which works on a link equivalently is estimated by introducing a disturbance observer[7] for the transfer part $P_k(s)$, instead of measuring by installing a force/moment sensor which may loose a feature of compactness. The estimated disturbance $D(s)(= -F_e(s))$ is transfered to the hand coordinate force/moment vector $\boldsymbol{f_m}$ through a transpose of Jacobian matrix J^T and then fed back by being multiplied with a compliance matrix $\boldsymbol{K}^{-1} = diag\{K_x^{-1}, K_y^{-1}, K_z^{-1}, K_\phi^{-1}, K_\theta^{-1}, K_\psi^{-1}\}^T$.

C. Detecting contact force and contact point

Fig.5 shows a geometrical model where contact force vector $\boldsymbol{f}$ is applying at a contact point represented by position vector $\boldsymbol{R} = [x_0, y_0, z_0]^T$. So the first purpose of this study is to detect these vector $\boldsymbol{f}$ and $\boldsymbol{R}$ based on the estimated force/moment vector $\boldsymbol{f_m}$.

Here we consider $\boldsymbol{f_m} = [\boldsymbol{f_t}^T, \boldsymbol{\tau}^T]^T$ with transient force vector $\boldsymbol{f_t}$ and moment one $\boldsymbol{\tau}$. As you see that, force vector $\boldsymbol{f}$ is simply derived from the balance of translational force around the origin as

$$\boldsymbol{f} = \boldsymbol{f_t} \tag{6}$$

In the mean while, if the equation of manipulator's surface is known as Eq.(7), then the contact point can be derived based on the balance of moment shown by Eq.(8) in the following manner[8].

$$g(x_0, y_0, z_0) = 0 \tag{7}$$

$$\boldsymbol{R} \times \boldsymbol{f} = \boldsymbol{\tau} \tag{8}$$

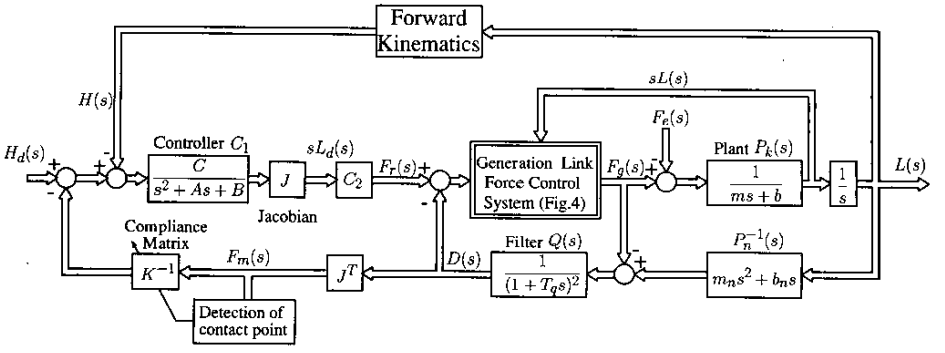

Fig. 3. Proposed compliance control system

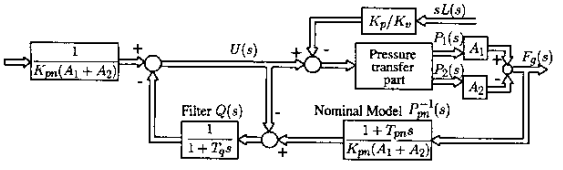

Fig. 4. Generation force control system

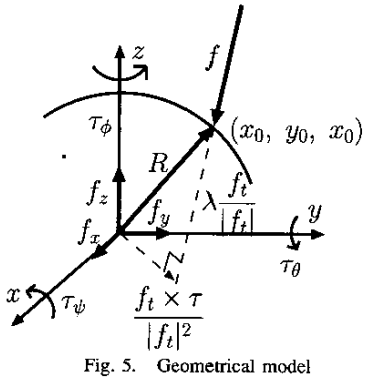

Fig. 5. Geometrical model

From Fig.5, position vector $\boldsymbol{R}$ can be described using a parameter λ as

$$\boldsymbol{R}=\frac{\boldsymbol{f_t}\times\boldsymbol{\tau}}{|\boldsymbol{f_t}|^2}+\lambda\frac{\boldsymbol{f_t}}{|\boldsymbol{f_t}|} \tag{9}$$

And $\boldsymbol{R}$ is obtained by substituting Eq.(9) into Eq.(7) to determine λ.

In our manipulator, as shown in Fig.1(a), a hemispherical shell, which is made of plaster, is introduced as the outer shape, whose center matches to the origin of $\boldsymbol{h}$.

Therefore giving an equation of hemispherical shell as Eq.(10) with radius r, contact point can be represented by Eq.(11), where $[x_1,\ y_1,\ z_1]^T$ is a first term of right hand side of Eq.(9).

$$x_0^2+y_0^2+z_0^2=r^2 \tag{10}$$

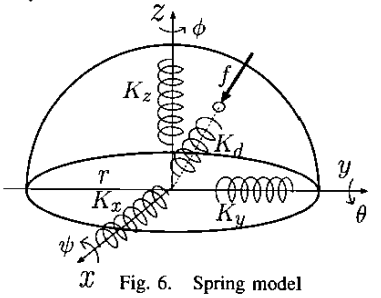

Fig. 6. Spring model

$$x_0 = x_1+f_x\sqrt{\frac{r^2-(x_1^2+y_1^2+z_1^2)}{f_x^2+f_y^2+f_z^2}} \tag{11.a}$$

$$y_0 = y_1+f_y\sqrt{\frac{r^2-(x_1^2+y_1^2+z_1^2)}{f_x^2+f_y^2+f_z^2}} \tag{11.b}$$

$$z_0 = z_1+f_z\sqrt{\frac{r^2-(x_1^2+y_1^2+z_1^2)}{f_x^2+f_y^2+f_z^2}} \tag{11.c}$$

In the next, displaying corresponding compliance to the contact point is considered. Fig.6 shows a geometrical compliance model, where K_d is a desired stiffness along with the direction of the contact point. Hence the remaining problem is how much each element K_x, K_y, K_z should be set to realize the desired stiffness K_d for any contact point.

From a balance of translational force at the origin of $\boldsymbol{h}$, the desired stiffness K_d for the direction of the contact point $(x_0,\ y_0,\ z_0)$ and the stiffness for each axis K_x, K_y, K_z satisfy the relation represented by Eq.(12), where $[\Delta x,\ \Delta y,\ \Delta z]^T$ is a displacement vector generated by an applied contact force. The left hand side corresponds to the desired force converted to the direction of contact point vector and the right one do the resultant force of each axis.

$$\left(K_d\frac{\Delta x\ x_0+\Delta y\ y_0+\Delta z\ z_0}{\sqrt{x_0^2+y_0^2+z_0^2}}\right)^2 = (K_x\Delta x)^2+(K_y\Delta y)^2+(K_z\Delta z)^2 \tag{12}$$

In order that K_x, K_y and K_z may satisfy Eq.(12), we introduce a constraint condition which makes the compliance control characteristic be normalized for each direction in the following manner. The closed loop relation of the control system shown in Fig.3 is described as

$$\boldsymbol{F_m} = \boldsymbol{I_{mp}} \boldsymbol{J}^T \boldsymbol{J} \boldsymbol{C_1} \boldsymbol{G_r}^{-1} (\boldsymbol{I} + \boldsymbol{I_{mp}} \boldsymbol{J}^T \boldsymbol{J} \boldsymbol{C_1} \boldsymbol{K}^{-1})^{-1} (\boldsymbol{H_d} \boldsymbol{G_r} - \boldsymbol{H}) \tag{13}$$

, where I_{mp} corresponds to a mechanical impedance in the velocity control loop(namely satisfying $sL = sL_d + I_{mp}F_e$ in Fig.3). In our manipulator, it is designed so that $\boldsymbol{J}^T\boldsymbol{J}$ may become almost diagonal at the origin of hand coordinate frame $\boldsymbol{h}$, which means that the relation between $\boldsymbol{F_m}$ and $(\boldsymbol{H_d G_r} - \boldsymbol{H})$ can be considered to be diagonal. The value of $\boldsymbol{J}^T\boldsymbol{J}$ at origin of $\boldsymbol{h}$ is represented by Eq.(15), where non-diagonal elements are denoted as 0 since they are thoroughly small compared to the diagonal one.

$$\boldsymbol{J}^T\boldsymbol{J} = \tag{14}$$

$$\begin{bmatrix} 1.5 & 0 & 0 & 0 & 0 & 0 \\ 0 & 1.5 & 0 & 0 & 0 & 0 \\ 0 & 0 & 2.9 & 0 & 0 & 0 \\ 0 & 0 & 0 & 3.0 \times 10^3 & 0 & 0 \\ 0 & 0 & 0 & 0 & 1.4 \times 10^3 & 0 \\ 0 & 0 & 0 & 0 & 0 & 1.4 \times 10^3 \end{bmatrix}$$

Seeing from Eq.(15), diagonal element corresponding to the z axis in $\boldsymbol{J}^T\boldsymbol{J}$ is almost 2 times as much as that for x and y axis. Therefore by setting each element of $\boldsymbol{K}$ according to the ratio in Eq.(15), the frequency characteristic between $\boldsymbol{F_m}$ and $\boldsymbol{H_d G_r} - \boldsymbol{H}$ for x, y, z direction becomes equivalent except for the influence of a static gain.

$$K_x : K_y : K_z = 1 : 1 : 2 \tag{15}$$

Substituting Eq.(15) into Eq.(12), desired stiffness for each axis is given as

$$K_x = \frac{K_d(\Delta x\ x_0 + \Delta y\ y_0 + \Delta z\ z_0)}{r\sqrt{\Delta x^2 + \Delta y^2 + 4\Delta z^2}} \tag{16.a}$$

$$K_y = \frac{K_d(\Delta x\ x_0 + \Delta y\ y_0 + \Delta z\ z_0)}{r\sqrt{\Delta x^2 + \Delta y^2 + 4\Delta z^2}} \tag{16.b}$$

$$K_z = \frac{2K_d(\Delta x\ x_0 + \Delta y\ y_0 + \Delta z\ z_0)}{r\sqrt{\Delta x^2 + \Delta y^2 + 4\Delta z^2}} \tag{16.c}$$

In this study, the stiffness for the rotational direction K_ϕ, K_θ, K_ψ are all set to be 0, which means positioning control is implemented for the rotational direction.

Fig.7 shows the frequency characteristic of the coefficient of $\boldsymbol{H_d G_r} - \boldsymbol{H}$ in Eq.(13). By normalizing the frequency characteristic of the compliance control performance for each axis, the frequency characteristic of the desired compliance (admittance) can be also prescribed by the same frequency characteristic, which is useful in evaluating the realization of the desired compliance (admittance) in a frequency domain.

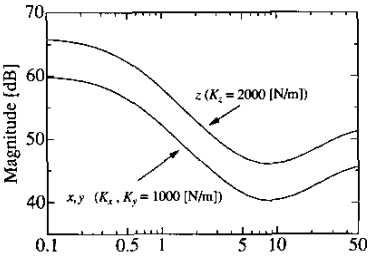

Fig. 7. Frequency characteristic

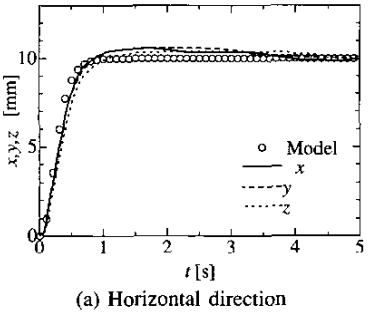

(a) Horizontal direction

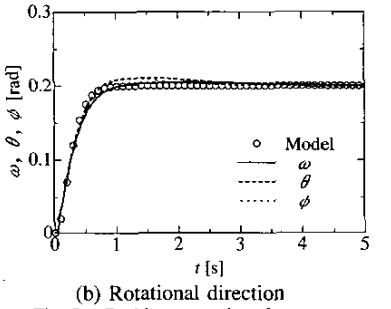

(b) Rotational direction

Fig. 8. Position control performance

IV. Experiments and Discussion

A. Position control performances

Fig.8 shows the positioning step response, where (a) and (b) corresponds to the horizontal and rotational direction, respectively. A small circle ∘ indicates the response of a model shown in Eq.(5), where parameters are chosen as $A = 38, B = 410, C = 1400$ in order that the step response may be almost the same with that of 2nd order system with $\omega_n = 8.0$ rad/s and $\zeta = 1.0$.

In the both figures, a little overshoot are confirmed but the obtained response for each direction is almost the same with that of the desired model, which proves an effectiveness of a proposed position control system.

B. Detection of contact force vector and contact point

Fig.9 shows the estimation performances of the contact force and contact point. Contact force is applied through a force sensor continuously 3 times for the same point (x_0, y_0, z_0)=(-21.4, 37.0, 74.0) [mm] as shown in the

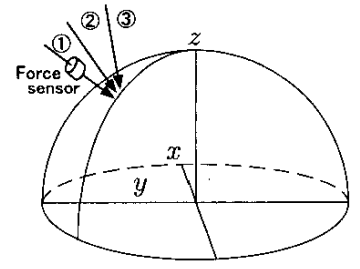

(a) Experimental situation

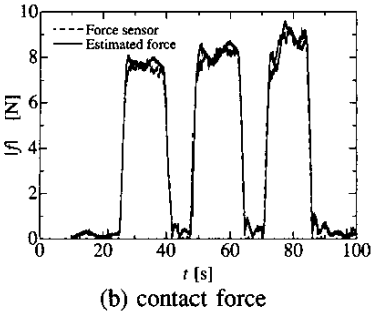

(b) contact force

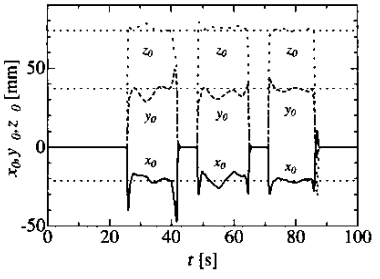

(c) contact point

Fig. 9. Estimation performance of contact force and contact point

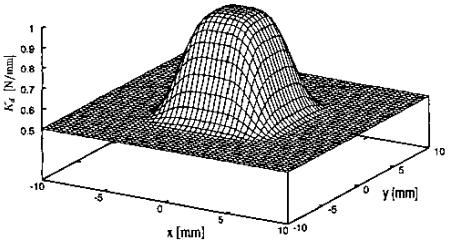

Fig. 10. Stiffness model

figure (a). The estimation performance of contact force and contact point are shown in (b) and (c), respectively. In spite that force is applied from various direction, both of the contact force and contact point can be confirmed to be estimated well, which proves the effectiveness of the proposed detection scheme.

C. Compliance display performance

Compliance displaying performances are verified. We introduce a geometrical model of a stiffness on a human skin as Eq.(17) approximately, which means reference

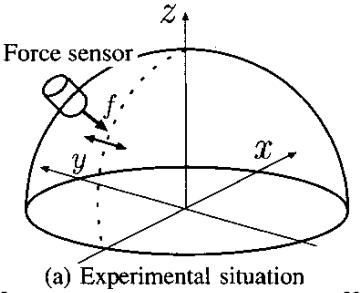

(a) Experimental situation

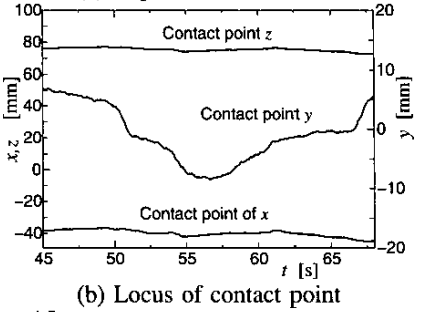

(b) Locus of contact point

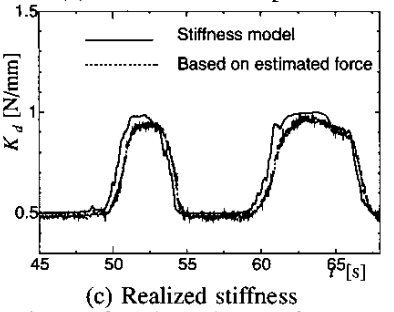

(c) Realized stiffness

Fig. 11. Compliance display performance

stiffness K_d displaying for a fingertip has a maximum value of K_{max} at a point $[x_p, y_p, z_p]$ and according to going away from that point K_d closes to the minimum one K_{min}.

$$K_d = (K_{max} - K_{min}) \times exp\{(-\frac{(x_0 - x_p)^4 + (y_0 - y_p)^4 + (z_0 - z_p)^4}{s_p})\} + K_{min} \quad (17)$$

Fig.10 shows the geometrical image of Eq.(17), where restriction of $z_0 = 0$ is introduced to make possible it to be shown in the actual 3-d space, where (x_p, y_p, z_p)=(0,0,0), K_{max} = 1.0[N/mm], K_{min}=0.5[N/mm], and spreading parameter $s_p = 200$.

Fig.11 shows the experimental result of compliance display by palpation motion. As shown in figure (a), human holds a force sensor and execute a round trip motion in order that contact point may go over the most rigid point with applying a force for normal direction continuously. The most rigid point is set to be (x_p, y_p, z_p)=(-

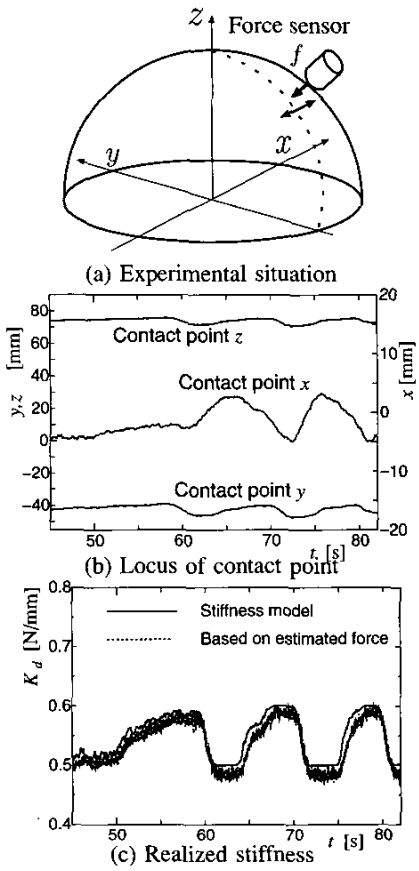

(a) Experimental situation

(b) Locus of contact point

(c) Realized stiffness

Fig. 12. Compliance display performance

40.0, 0.0, 75.5)[mm] and the stiffness is determined as $K_{max} = 1.0$ [N/mm], $K_{min} = 0.5$ [N/mm] based on the prior measurement stiffness data of a forearm.

Fig.11 (b) shows the locus of the contact point. Seeing from the figure, round trip motion is confirmed to be done for the direction along with y axis.

Fig.11 (c) shows the realized stiffness, where solid line corresponds to the value obtained from a models shown in Eq.(17), while dotted one indicates the actual realized stiffness obtained by a calculation of $|f_t|/\sqrt{(\Delta x)^2 + (\Delta y)^2 + (\Delta z)^2}$.

A response lag can be confirmed, which is considered to be resulted from dynamics lag of inner position control system, but almost satisfactory displaying property can be obtained, which proves that the proposed displaying scheme works properly. Further improvement of the displaying performance is the matter to be settled at present.

Fig.12 shows the same experimental results with Fig.11 except that the difference stiffness $K_{max} - K_{min}$ is quite small of 0.1 [N/mm] for the contact point of (x_p, y_p, z_p)=(0.0, -40.0, 75.5)[mm]. It is confirmed that even small variation of stiffness of 0.1 [N/mm] can be displayed, which is owing to the air compressibility and it is the advantage of employing a pneumatic driving system.

V. Conclusion

In this study, we developed a mechanical system using a pneumatic parallel manipulator, aiming at displaying a compliance characteristic on a human skin.

In order to realize such a motion, we proposed a compliance displaying scheme, where a contact point(which point on the surface of the device an operator is touching at) and contact force(how much force an operator is applying) are detected using an estimated force/moment with no use of general force/moment sensor and then display the target compliance determined according to the contact point by constructing a compliance control system.

Through some experiments, almost satisfactory control performances can be confirmed both in estimating contact force and contact point and in displaying the reference stiffness. The small variation of stiffness of 0.1 [N/mm] can be displayed, which is owing to the air compressibility of pneumatic actuator.

In addition to the further improvement of compliance displaying performance, the concrete recognition using not only sense of force feeling reported here but that of vision by constructing the deseased part in a computer using graphics image is under the current investigation.

VI. References

[1] J.Kim,S.De,Slinivasan, "Computationally efficient techniques for real time surgical simulation with force feedback", *Proc. 10th Symp. on Haptic Interface for Virtual Environment and Teleoperator Systems, HAPTICS 2002*, 2002, pp.51-57

[2] S.Majima and K.Matsushima, "Fuzzy Evaluation of Stiffness of Tissue by means of Micro-manipulator", *Proc. SPIE- Int. Soc. Opt. Eng. (USA)*, Vol.2101, No.1, 1993, pp. 521-526,

[3] M. Takaiwa and T. Noritsugu, "Development of Pneumatic Human Interface and Its Application to Compliance Display", *J. of Robotics and Mechatronics*, Vol.13, No.5,2001,pp.472-478

[4] D.Stewart, "A platform with Six Degrees of Freedom", *Proc. Inst. Mechanical Engineers*,180-15,1965,pp.371-386

[5] D.McCloy and H.R.Martin, "Control of Fluid Power: Analysis and Design", *2nd (Revised) Edition, (1980), pp.339*, John Wiley& Sons

[6] T. Noritsugu and M. Takaiwa, "Motion Control of Pneumatic Parallel Manipulator Using Disturbance observer", *Japan-U.S.A. Flexible Automations*, 1986

[7] T. Murakami and K. Ohnishi, "Advanced Control Technique in Motion Control", *The Nikkan Kogyo Shinbun Ltd., Japan*, 1990

[8] J.K.Salisbury, Jr., "Interpretation of Contact Geometries from Force Measurements", *Proc.of 1st Int. Symp. on Robotics Research(MIT Pewss)*,pp.565-577, 1984